RESEARCH ARTICLE

Decreases in the urban heat island effect during the Coronavirus Disease 2019 (COVID-19) lockdown in Wuhan, China: Observational evidence

Sun Shanlei[1] | Zhou Decheng[2] | Chen Haishan[1] | Li Jinjian[3] |
Ren Yongjian[4] | Liao Hong[5] | Liu Yibo[2]

[1]Collaborative Innovation Center on Forecast and Evaluation of Meteorological Disasters/Key Laboratory of Meteorological Disaster, Ministry of Education/International Joint Research Laboratory on Climate and Environment Change, Nanjing University of Information Science & Technology (NUIST), Nanjing, China

[2]School of Applied Meteorology, Nanjing University of Information Science & Technology (NUIST), Nanjing, China

[3]School of Atmospheric Sciences, Chengdu University of Information Technology, Chengdu, China

[4]Regional Climate Center of Wuhan, Wuhan, China

[5]Jiangsu Key Laboratory of Atmospheric Environment Monitoring and Pollution Control/Collaborative Innovation Center of Atmospheric Environment and Equipment Technology, Nanjing University of Information Science & Technology (NUIST), Nanjing, China

Correspondence
Sun Shanlei, Collaborative Innovation Center on Forecast and Evaluation of Meteorological Disasters, Nanjing University of Information Science & Technology (NUIST), Nanjing 210044, China.
Email: sun.s@nuist.edu.cn

Abstract

The Coronavirus Disease 2019 (COVID-19) lockdown in early 2020 reduced human activities in Wuhan, China, thereby altering the urban heat island (UHI) effect. The epidemic period (EP) during January 1, 2020–May 31, 2020 is divided into four stages, including pre-lockdown, first (EP_LS1) and second (EP_LS2) lockdown, and after-lockdown (EP_ALS) stages, which are identified according to different antivirus measures in early 2020 and confirmed by comparing the daily electricity consumption over the Wuhan metropolitan area during 2020 and 2019. Then, the Wuhan UHI intensity (UHII) during each stage is compared to that during the baseline period of 2016–2019 and 2021. Daytime, night-time, and daily UHIIs are reduced; the larger decrease is during EP_LS1 and EP_LS2, of which EP_LS1 with the strictest antivirus measures shows a significant decrease ($<-0.12°C$ or $<-36\%$), especially during night-time with $-0.23 \pm 0.05°C$ (or $-47 \pm 9\%$). The declined UHII persists in all stages (excluding EP_ALS), even after removing the natural variability of the air temperature; EP_LS1 still exhibits the largest and significant decrease ($<-0.18°C$ or $<-52\%$). To remove possible impacts of the local weather conditions, the UHII changes are recalculated by randomly sampling the 90, 80, 70, and 60% data points in each stage of EP with 1,000 repetitions. Results suggest limited influence of the local weather conditions, and then validate our findings. This study provides an important observational evidence of human-induced control on urban climate, and further confirms the necessity to include human dynamics in climate/earth system models for better simulating and predicting urban climate.

KEYWORDS
COVID-19 lockdown, human activities, urban heat island, Wuhan

1 | INTRODUCTION

In early December 2019, the abrupt outbreak of the Coronavirus Disease 2019 (COVID-19) occurred in Wuhan, China, and spread rapidly across the globe (Wang and Zhang, 2020; Yang et al., 2020a). As of February 2021, there had been more than 27 million confirmed cases globally, with more than 2.1 million deaths (Word Health Organization (WHO), 2021). For preventing the rapid COVID-19 spread across China, drastic measures were implemented, including a nationwide lockdown in late January 2020 (Tian et al., 2020). Specifically, the government closed the outbound corridors of Wuhan on January 23, 2020, limited vehicle use, and closed schools, government offices, and factories (Chen et al., 2020; China Internet Information Center, 2020; Hubei Government, 2020).

China's antivirus measures have inconvenienced personal daily life and society operation and have led to sizable socio-economic losses (Wang and Zhang, 2020); nevertheless, the nationwide lockdown constitutes an ideal and unprecedented opportunity for researching human activities and related impacts. The nationwide lockdown likely resulted in decreased air pollutant emissions across China. Analysing the altered emissions of these pollutants and elucidating the underlying mechanisms has become a cutting-edge research topic in 2020 (e.g., Chen et al., 2020; Hubei Government, 2020; Miyazaki et al., 2020; Shi and Brasseur, 2020; Yang et al., 2020a). Wang and Zhang (2020) showed that relative to the reference years 2012–2018, China's average $PM_{2.5}$ (particulate matter <2.5 μm diameter) and PM_{10} (particulate matter <10 μm diameter), and SO_2, CO, and NO_2 concentrations were remarkably reduced during the 2020 lockdown while the O_3 concentration increased. Aerosols have a cooling effect on the atmosphere, which is induced directly by scattering and absorbing solar radiation, and indirectly by altering cloud properties (Chistoforou et al., 2000; Wu et al., 2017; Yang et al., 2020a; 2020b); hence, declined aerosol emissions during the COVID-19 lockdown would lead to an increase in air temperature. Yang et al. (2020a) showed that in January–March 2020, an anomalous warming of 0.05–0.15 K was apparent in eastern China under different scenarios of reduced aerosol emissions.

Besides the aerosol response to the strict antivirus measures (e.g., quarantine, closed social services, and limited vehicle use), the anthropogenic heat (AH) released due to human activities also decreased. AH is associated with the urban energy balance; hence, it likely impacts the urban heat island (UHI) effect (Tong et al., 2004; Fan and Sailor, 2005; Narumi et al., 2009; Oleson et al., 2011; Feng et al., 2012; Varentsov et al., 2018; Raj et al., 2020), according to which land surface and/or air temperatures are higher in urban areas than in rural surroundings (e.g., Oke, 1982;

Arnfield, 2003; Ren et al., 2007; Narumi et al., 2009; Raj et al., 2020; Oleson et al., 2011; Gedzelman et al., 2013; Chen et al., 2014; Zhou et al., 2014; Zhang et al., 2015a; 2015b; Varentsov et al., 2018). Based on a boundary-layer model with an AH emission inventory for Beijing, Tong et al. (2004) showed that daytime and night-time UHI intensity (UHII) in winter increased by ∼0.5 and 1–2°C due to AH, respectively. Fan and Sailor (2005) used a mesoscale atmospheric model to simulate the AH impact on the urban climate of Philadelphia, PA, and pointed out that AH could contribute 2–3°C to the night-time UHII. Varentsov et al. (2018) analysed the AH impact on UHII during heavy winter conditions in Apatity City, Russian Federation, and stated that AH warmed the city by ∼1 K on average in winter; during extremely cold days, AH warmth contributed up to 6 K in the city centre.

Numerous studies have addressed the impact of reduced human activities during the COVID-19 lockdown on air quality across the world (e.g., Goldberg et al., 2020; Miyazaki et al., 2020; Turner et al., 2020; Wang and Zhang, 2020). To date, it is still unclear how the UHI effect responds to the COVID-19 prevention and control measures, and the magnitude of its changes. Here, we examine the daytime, night-time, and daily UHII changes in Wuhan of China between January 1, 2020 and May 31, 2020 (relative to the baseline 2016–2019 period) with a focus on impacts of the antivirus measures, allowing us to separate human influence on urban climate, particularly due to the AH reductions. Therefore, the evaluations of the UHII changes in the COVID-19 lockdown provide an important reference for quantitatively understanding human-induced control on urban climate, which is helpful for optimally managing and utilizing the UHI effect and enhancing residential quality in urban areas. Moreover, the findings will further confirm the necessity to include human dynamics in climate/earth system models for better simulating and predicting urban and even local climate (Oleson et al., 2011; Donges et al., 2020; Beckage et al., 2018; Turner et al., 2020).

2 | STUDY AREA, DATA, AND METHODOLOGY

2.1 | Study area

Wuhan, the commercial and administrative capital city of Hubei Province, China, has direct jurisdiction over 13 districts between 29°58′–31°22′N and 113°41′–115°05′E (enclosed by red line in Figure 1). A humid, subtropical climate prevails in this region, with distinct seasons, abundant rainfall, intense sunshine, and extremely muggy summer weather, which is why Wuhan is referred to as one of
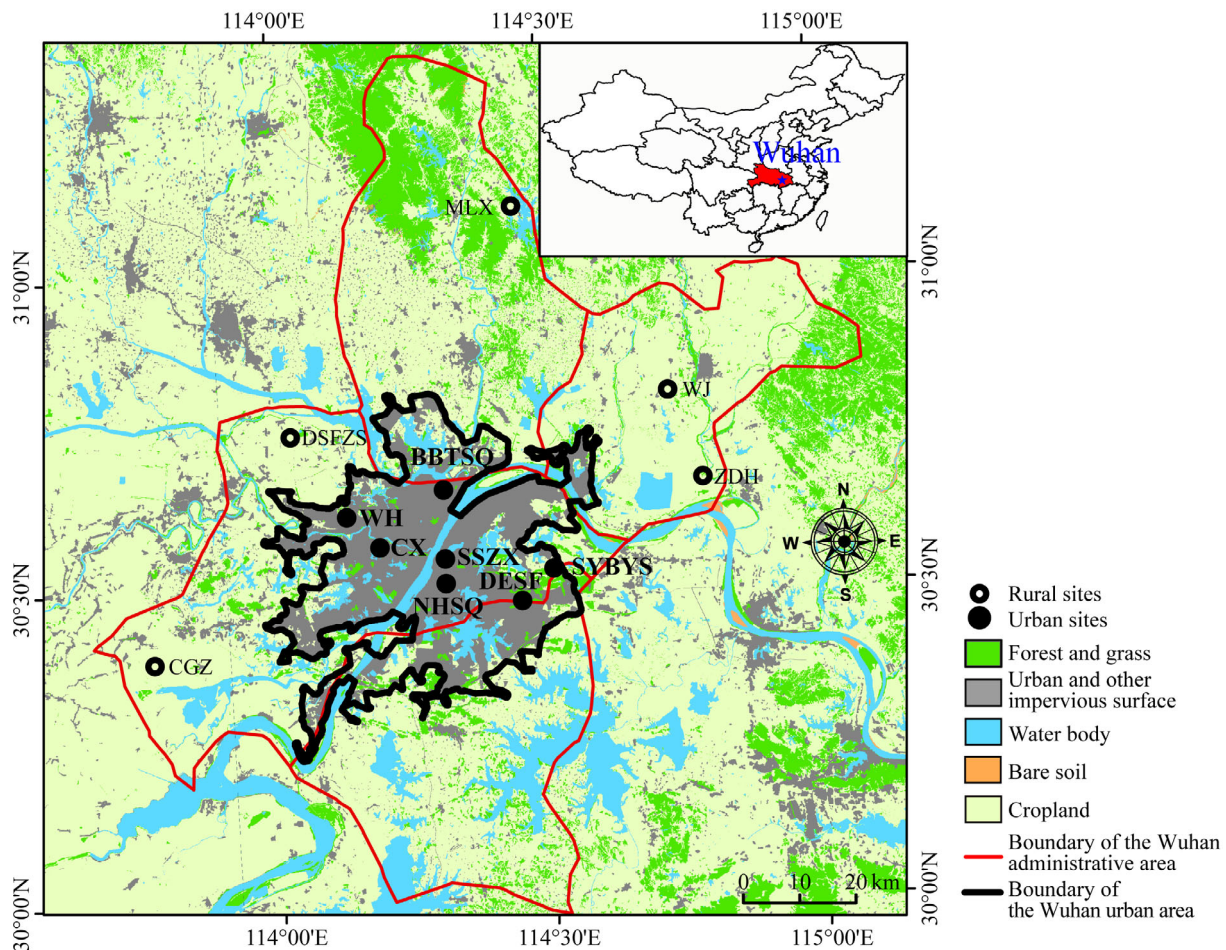
FIGURE 1 Major land-surface classifications and the selected 11 meteorological sites around Wuhan, China. Bold indexes are the abbreviated names of the urban sites (see Tables S1 and S2)

China's "Three Furnaces." Wuhan has a vast plain with the Yangtze and Han Rivers crossing the city and is surrounded by hills in the south and north. Lakes and ponds in Wuhan constitute more than a quarter of the urban area. Here, we focus on the main urban area (enclosed by black bold line in Figure 1) rather than the wider metropolitan area.

2.2 | Data

Due to different construction times of the high-density autonomous weather sites in Wuhan, the time spans of the observed hourly 2-m air temperature differed among sites, and the spatial coverages of the sites varied with years. Therefore, to maximize the utilization of the observed air temperature dataset, we first selected 119 meteorological sites from the Wuhan Regional Climate Center of Hubei Meteorological Bureau (HMB), which corresponded to a time span of observations between January 1 and May 31, 2016–2021. The HMB has conducted quality control and

eliminated possible erroneous measurements using a regional climatological extreme value method (Yang et al., 2011; Oleson, 2012; Yang and Liu, 2013). The sites with missing values exceeding 5% of the total records during the study period were removed, and eventually, 47 sites remained. Missing hourly values in these sites were supplemented with data from neighbouring sites using a linear regression technique.

The urban and rural areas were identified using a spatial buffer analysis (Zhou et al., 2014) based on the 30 × 30 m GlobeLand30 dataset of 2020 (http://www.globallandcover.com/; Chen et al., 2014) (details in Data S1, Supporting Information). We first categorized the 47 sites into 17 urban and 30 rural candidate sites. Then, the procedure for identifying the urban and rural sites is as follows (Jia et al., 2021): (a) We defined different buffer zones at radii of 1, 2, 3, 4, 5, 7, ..., and L km ($L = 78$ here; representing the long side of a rectangle covering the Wuhan urban area) from each site. The corresponding area percentages of built-up land in each buffer zone were calculated based on the 2020

GlobeLand30 dataset. (b) When the percentage of built-up land areas within the 1–5 and 7–78-km buffer zones of a rural candidate site was less than 3 and 15%, respectively, this candidate site was identified as a rural site. In contrast, if the percentage of built-up land areas within the 1–5-km buffer zones of an urban candidate site was more than 70%, this site was identified as an urban site. (c) Sites less than 1 km from 2020 GlobeLand30 water bodies were removed, and the absolute differences in the average elevations between rural and urban sites should be smaller than 30 m. (d) Google Earth was used for visual comparisons between 2016 and 2020 (Figures S1 and S2) to minimize the impact of land cover changes on the UHI. Sites showing obvious changes in land cover within a 100-m radius were also removed. Eventually, four rural and seven urban sites were selected (Figure 1), and their information, including latitude, longitude, elevation, instrument, temperature sensor, and sampling frequency, can be found in Tables S1 and S2.

The daytime and night-time air temperatures were estimated by averaging the hourly values between 0600 and 1700 Local Solar Time (LST, UTC + 8) and between 1800 and 0500 LST, respectively. The average of the daytime and night-time temperatures was defined as the daily temperature. Additionally, the daily electricity consumption data for the Wuhan metropolitan area (enclosed by the red line in Figure 1) during 2019 and 2020 were collected from Wuhan Power Supply Company, which will indirectly show the curtailment of residential activities during the COVID-19 lockdown in 2020. The air temperature averaged over the urban (rural) sites represents the urban (rural) basic condition; this distinction minimizes local influences on air temperature that may be particular to one site.

2.3 | Methodology

To quantify the COVID-19 impact on the Wuhan UHI effect, we have firstly divided the period January 1, 2020–May 31, 2020 (i.e., EP) into four stages according to antivirus measures (China Internet Information Center, 2020; Hubei Government, 2020): pre-lockdown stage (i.e., EP_PLS; January 1–22) with no or loose antivirus measures; first lockdown stage (i.e., EP_LS1; January 23–March 19) with the strictest antivirus measures (e.g., closed outbound corridors of Wuhan, schools, government offices, and factories); second lockdown stage (i.e., EP_LS2; March 20–April 28) with strict antivirus measures (e.g., Wuhan lockdown) still in effect and some social sectors (i.e., factories) reopened; and after-lockdown stage (i.e., EP_ALS; April 29–May 31) with lift of the Wuhan lockdown and return of most human activities to normal levels. Correspondingly, the baseline period (i.e., BP) between January 1–May 31, 2016–2019 and 2021 was also divided into the respective four stages, that is, BP_PLS, BP_LS1, BP_LS2, and BP_ALS. Daytime, night-time, and daily air temperatures for each BP stage were averaged over 2016–2019 and 2021. Despite of limited data of daily electricity consumption over the Wuhan metropolitan area, the large negative anomaly during January 22, 2020–April 28, 2020 (relative to the corresponding period of 2019) strongly suggests that the antivirus measures did play a role in reducing human activities, especially for EP_LS1 (Figure S3), in which the strictest antivirus measures were implemented.

In this study, the UHII is defined as urban (T_U) minus rural (T_R) temperatures (e.g., Oke, 1982; Ren et al., 2007). Thus, relative to BP, the change in UHII on the ith day of EP (i.e., $\Delta UHII^{EP-i}$) is

$$\Delta UHII^{EP\_i} = UHII^{EP\_i} - UHII^{BP_i}, \qquad (1)$$

where the superscripts of BP_i and EP_i represent the ith day of BP and EP, respectively.

The crux of estimating the effects of the lockdown on $\Delta UHII$ was to obtain T_U during EP with assumption of no anti-virus measures (i.e., human activities remaining at the level of BP; denoted by $\widehat{T}_U^{EP}$). To this end, we estimated $\widehat{T}_U^{EP}$ anomalies relative to the T_U averaged during BP, similar to Fujibe (2020). The basic considerations of this method are as follows: (a) Urban and rural areas share the same climate background (e.g., the same natural variability of the atmosphere). (b) During BP, T_U anomalies can be expressed as a certain function (i.e., a linear function) of T_R anomalies (relative to the T_R averaged during BP). (c) The BP relationship between T_U and T_R anomalies can be applied to EP. Considering the relationship mentioned above between daytime and night-time and in the BP stages, we developed the daytime and night-time equations for each stage based on multiple regression techniques and took the T_R anomalies of all rural sites as independent variables. The regression coefficients and verification results are presented in Table S3 and Figure S4, respectively. Overall, both daytime and night-time fluctuations of T_U anomalies during the BP stages closely agree with the estimated anomalies, with correlation coefficients of approximately 0.99 and mean biases of nearly zero. Therefore, the multiple regression equations are sound for estimating the T_U anomalies. Using these multiple regression equations, we calculated the daytime and night-time $\widehat{T}_U^{EP}$ anomalies, and $\widehat{T}_U^{EP}$ by adding the multi-year average of T_U^{BP}. Moreover, the daily $\widehat{T}_U^{EP}$ during EP was calculated with the mean of daytime and night-time values.

During EP, the corresponding UHII changes on the ith day of EP (i.e., $\Delta UHII_N^{EP\_i}$) can be expressed as

$$\Delta UHII_N^{EP\_i} = \underbrace{\left(\widehat{T}_U^{EP\_i} - T_R^{EP\_i}\right)}_{adUHII^{EPi}} - UHII^{BPi}, \qquad (2)$$

where $adUHII^{EP\_i}$ represents UHII at the ith day of EP, regardless of the lockdown impacts (i.e., human activities remaining at the level of BP). Thus, $\Delta UHII_N^{EP\_i}$ depends on the changes in natural atmospheric variability during EP relative to BP UHII. Correspondingly, the lockdown-induced UHII change on the ith day of EP (i.e., $\Delta UHII_H^{EP\_i}$) is obtained by

$$\Delta UHII_H^{EP\_i} = \Delta UHII^{EP\_i} - \Delta UHII_N^{EP_i}. \qquad (3)$$

With Equations (1)–(3), we obtained the time series of daytime, night-time, and daily $UHII^{EP\_i}$, $UHII^{BP\_i}$, $adUHII_N^{EP\_i}$, and $\Delta UHII_H^i$, which were subsequently used to check the significance ($p < .05$) of $\Delta UHII$ (i.e., mean of $\Delta UHII^{EP\_i}$ during each EP stage), $\Delta UHII_N$ (i.e., mean of $\Delta UHII_N^{EP\_i}$ during each EP stage), and $\Delta UHII_H$ (i.e., mean of $UHII_H^{EP\_i}$ during each EP stage) using a two-tailed Student's t test. Additionally, we calculated the relative $\Delta UHII$, $\Delta UHII_N$, and $\Delta UHII_H$ in each EP stage, which could be calculated by dividing by UHII in the corresponding stage of 2016–2021.

Although the method above can detach the impacts of natural variability of the atmosphere on $\Delta UHII$, the local weather conditions (i.e., wind speed, precipitation, cloud cover, etc.) are not reasonably addressed. Previous studies (Kistler et al., 2001; Arnfield, 2003; Yang et al., 2019) documented that local weather conditions were closely associated with energy fluxes and affected UHII. Therefore, the local weather conditions are expected to influence the estimated $\Delta UHII$, $\Delta UHII_N$, and $\Delta UHII_H$. However, the lack of data on wind speed, precipitation, and cloud cover makes it difficult to exclude data points that correspond to changes in local weather conditions during BP and EP. Therefore, the robustness of the detected $\Delta UHII$, $\Delta UHII_N$, and $\Delta UHII_H$ in EP in Wuhan would likely weaken. To clarify whether local weather conditions could influence our results, we randomly took the 90, 80, 70, and 60% data points from the UHII, $UHII_N$ and $UHII_H$ time series of each stage during BP and EP with 1,000 repetitions to recalculate $\Delta UHII$, $\Delta UHII_N$, and $\Delta UHII_H$. If the recalculated $\Delta UHII$, $\Delta UHII_N$, and $\Delta UHII_H$ do not noticeably change at a given stage and the occurrences of significant ($p < .05$) values among the 1,000 repetitions exceed 500, we conclude that local weather conditions have limited impact on the robustness of our analysis.
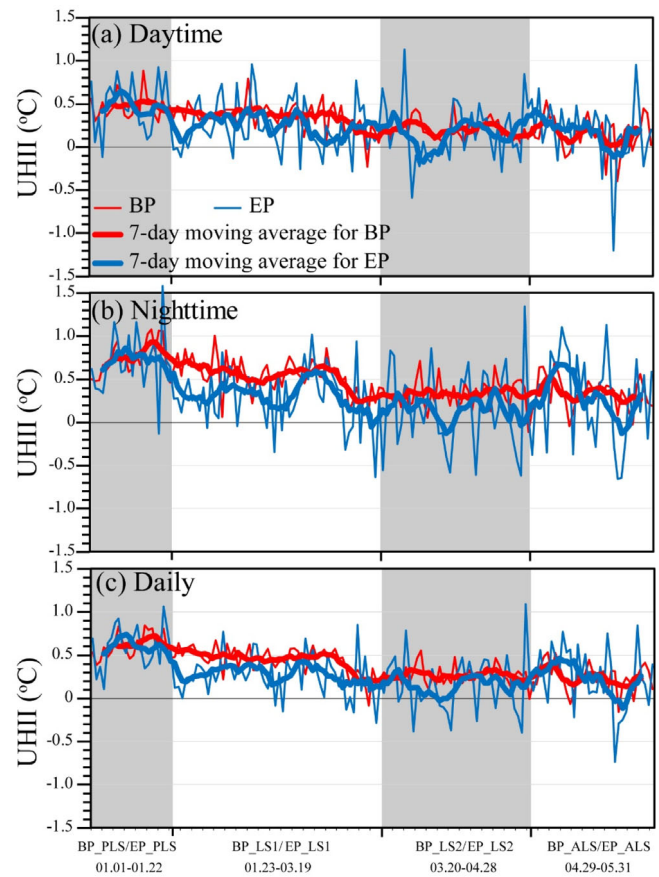

FIGURE 2 Time series of daytime (a), night-time (b), and daily UHII (c) during BP and EP, accompanied with the 7-day moving average

3 | RESULTS

3.1 | Characteristics of the Wuhan UHI effect during BP and EP

Figure 2 shows that values of daytime, night-time, and daily UHII during BP and EP are generally positive, and the values averaged in each stage of BP and EP are also positive (Figure 3a1–a3). These suggest that the UHI effect exactly exists in Wuhan, although there are large fluctuations from day to day and from stage to stage, mainly resulting from the seasonal variations in weather patterns and anthropogenic heating (Magee et al., 1999; Yow, 2007; Gedzelman et al., 2013). The daytime (daily) UHII gradually decreases from $0.48 \pm 0.04°C$ (mean ± 1 SE; $0.61 \pm 0.03°C$) in BP_PLS to $0.15 \pm 0.03°C$ ($0.25 \pm 0.03°C$) in BP_ALS, while the night-time UHII exhibits non-monotonic changes; that is, it first decreases from a maximum of $0.74 \pm 0.04°C$ in BP_PLS to a minimum of $0.33 \pm 0.03°C$ in BP_LS2, and subsequently increases. The night-time UHII is stronger than daytime UHII for all BP stages; the largest differences are above $0.26°C$ in BP_PLS. The major UHII characteristics
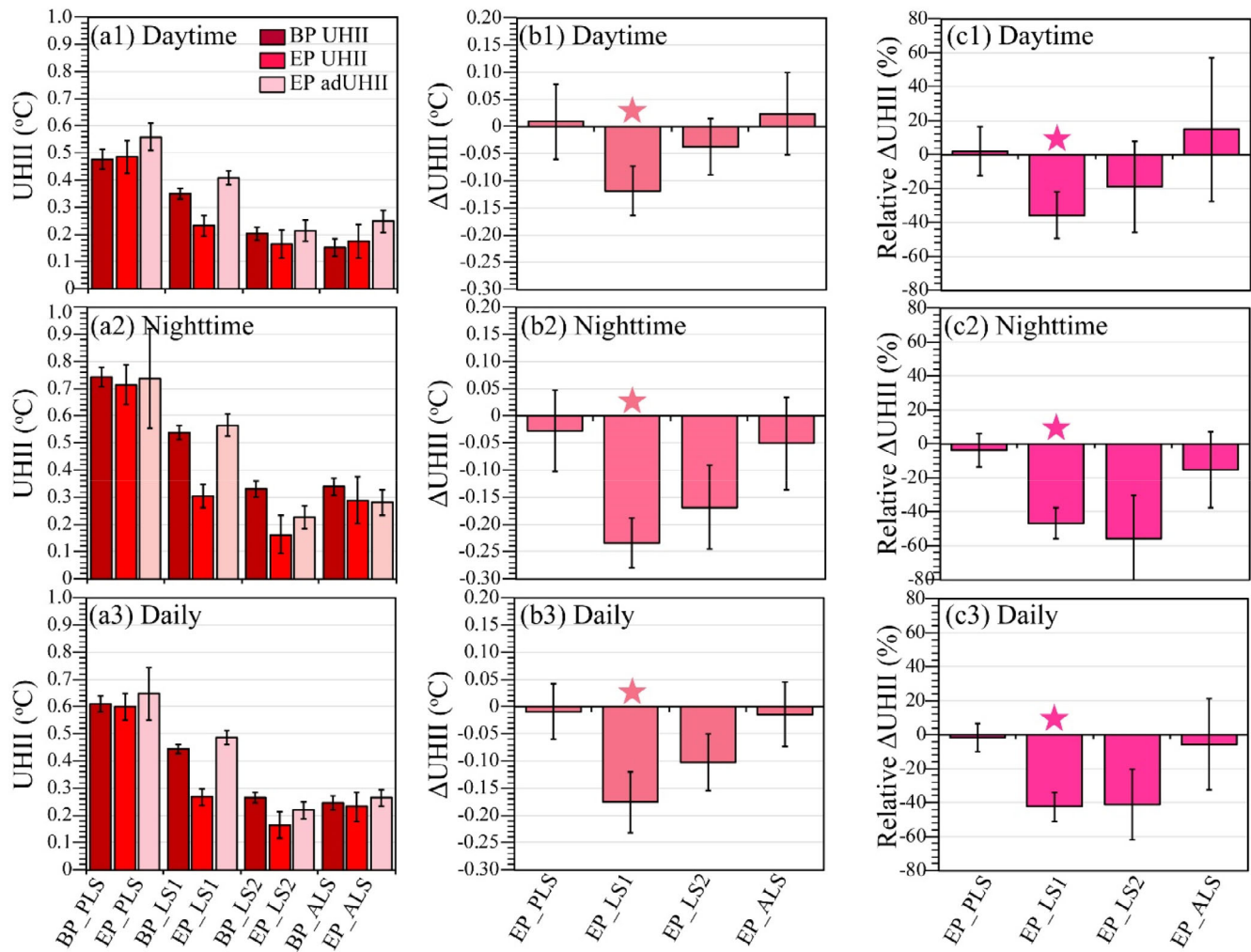
FIGURE 3 UHII and adUHII (a1–a3), ΔUHII (b1–b3) and relative ΔUHII (c1–c3) at four BP and EP stages. Stars indicate significant ($p < .05$) ΔUHII, and error bars are ±1 standard error (*SE*). The samples for BP_PLS, BP_LS, BP_LS2, and BP_ALS (EP_PLS, EP_LS, EP_LS2, and EP_ALS) are 22, 56, 40, and 33, respectively

during EP are different from those during BP (Figure 3a1–a3). For example, daytime, night-time, and daily UHII in EP exhibit consistent fluctuations from EP_PLS to EP_ALS; that is, they decrease to their minimum values (0.17 ± 0.05, 0.16 ± 0.07, and $0.16 \pm 0.05°C$ in daytime, night-time, and daily, respectively) in EP_LS1 and subsequently increase. Compared to the daytime UHII, the night-time UHII is stronger for all EP stages, followed by the largest difference of $0.23°C$ in EP_PLS.

3.2 | Changes in EP UHII compared to BP

To quantify the EP UHI effect variations relative to BP, the ΔUHII and the relative values at each EP stage are calculated. Subsequently, significance is tested with a two tailed Student's *t* test ($p < .05$; Figure 3b1–b3, c1–c3). The

UHII at each EP stage (excluding daytime EP_PLS and EP_ALS, and daily EP_PLS) declines in different ways. Seen from daytime, night-time, and daily ΔUHII, the largest and most significant ($p < .05$) reductions are below $-0.12°C$ at EP_LS1, especially during night-time with $-0.23 \pm 0.05°C$, while the values of the other three stages are above $-0.17°C$ (Figure 3b1–b3). Despite differences in magnitudes of the daytime, night-time, and daily UHII among the four BP stages, the fluctuations of relative ΔUHII are generally consistent with those of ΔUHII during EP, and EP_LS1 corresponds to the largest and most significant ($p < .05$) declines by below -36%, particularly for night-time with $-47 \pm 9\%$ (Figure 3c1–c3).

Regardless of the lockdown impacts during EP (i.e., human activities remaining at the level of BP), the EP UHII (i.e., adUHII) are shown in Figure 3a1–a3. Relative to the UHII during BP, the EP UHII still shows differences, mainly due to the differences in T_R between EP
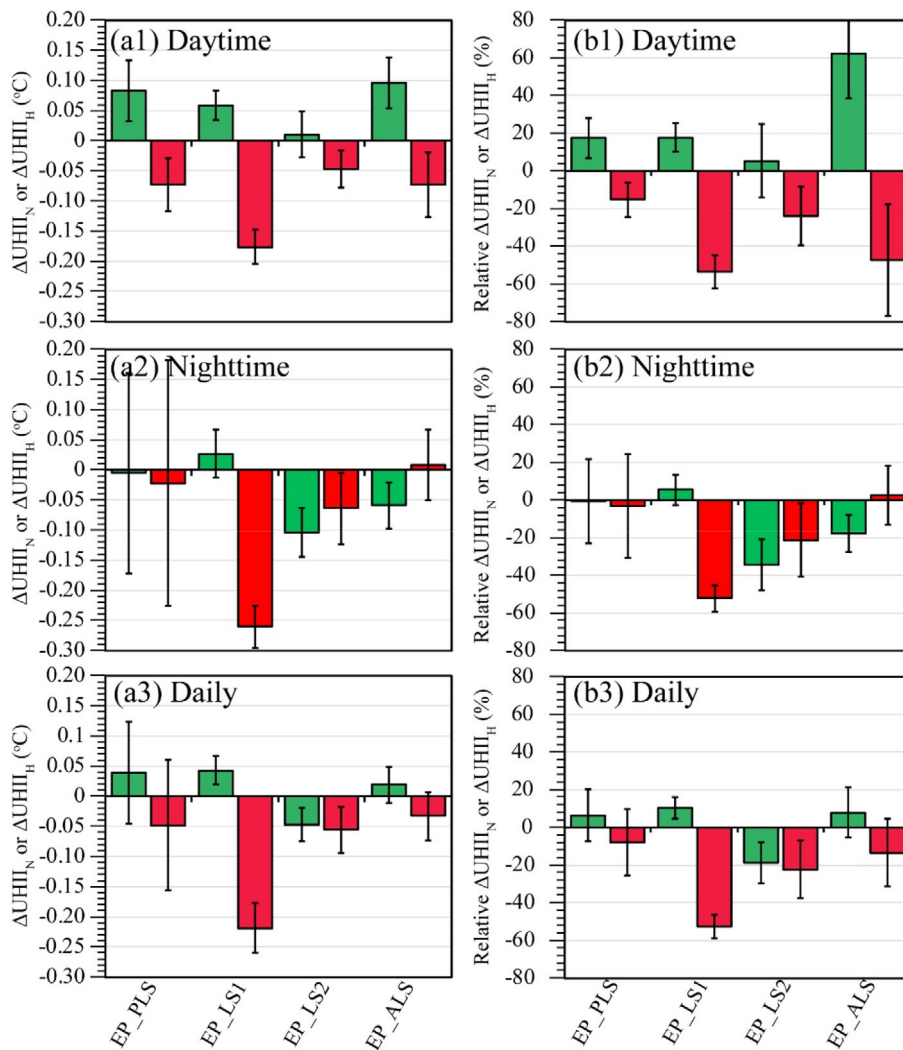
FIGURE 4 $\Delta UHII_N$ and $\Delta UHII_H$ (a1–a3), and their relative values (b1–b3) for each EP stage. Stars indicate significant ($p < .05$) values, and error bars are ± 1 standard error (*SE*). The samples for EP_PLS, EP_LS, EP_LS2, and EP_ALS are 22, 56, 40, and 33, respectively

and BP. Therefore, for measuring the impacts of T_R changes on $\Delta UHII$, we divided $\Delta UHII$ during each EP stage into $\Delta UHII_N$ and $\Delta UHII_H$ based on Equations (2) and (3) (Figure 4). $\Delta UHII_N$ indicates that its daytime values are positive at all EP stages and above 0.01°C, while the night-time values are generally negative and below −0.01°C during EP. By contrast, daily $\Delta UHII_N$ values are above 0.02°C during EP_PLS, EP_LS1, and EP_ALS, but equal to −0.05°C during EP_LS2. These results suggest that, due to the natural variability of air temperature, $\Delta UHII$ changed during EP, and therefore it is necessary to remove $\Delta UHII_N$ from $\Delta UHII$ for quantifying the impacts of the reduced human activities on the EP UHII changes. Despite somewhat differences in magnitudes of $\Delta UHII_H$ and $\Delta UHII$ during EP_LS1 and EP_LS2, the consistent signs of daytime, night-time, and daily values, suggest that the EP UHII dose change in response to human activities (Figure 4). Moreover, the smaller rates of EP_PLS and EP_ALS change, which correspond to inadequate prevention and control measures,

indicate limited impacts of human activities on UHII; however, the larger decreasing rates ($<−0.05$°C or $<−21$%) of EP_LS1 and EP_LS2 indicate that the UHII could indeed be reduced by strict antivirus measures. Especially, the daytime, night-time and daily EP_LS1 $\Delta UHII_H$ (the relative values) are significant ($p < .05$), respectively corresponding to $−0.18 \pm 0.03$°C ($−54 \pm 9$%), $−0.26 \pm 0.04$°C ($−52 \pm 7$%), and $−0.22 \pm 0.04$°C ($−53 \pm 6$%). Comparing $\Delta UHII_N$ and $\Delta UHII_H$, we found that except for EP_PLS and EP_ALS, decreases in the daytime, night-time, and daily UHII during EP_LS1 and EP_LS2 could be attributed to reduced human activities.

3.3 | Possible impacts of local weather conditions

To remove possible impacts of the local weather conditions (i.e., wind speed, precipitation, cloud cover, etc.), $\Delta UHII$, $\Delta UHII_N$, and $\Delta UHII_H$ were recalculated by
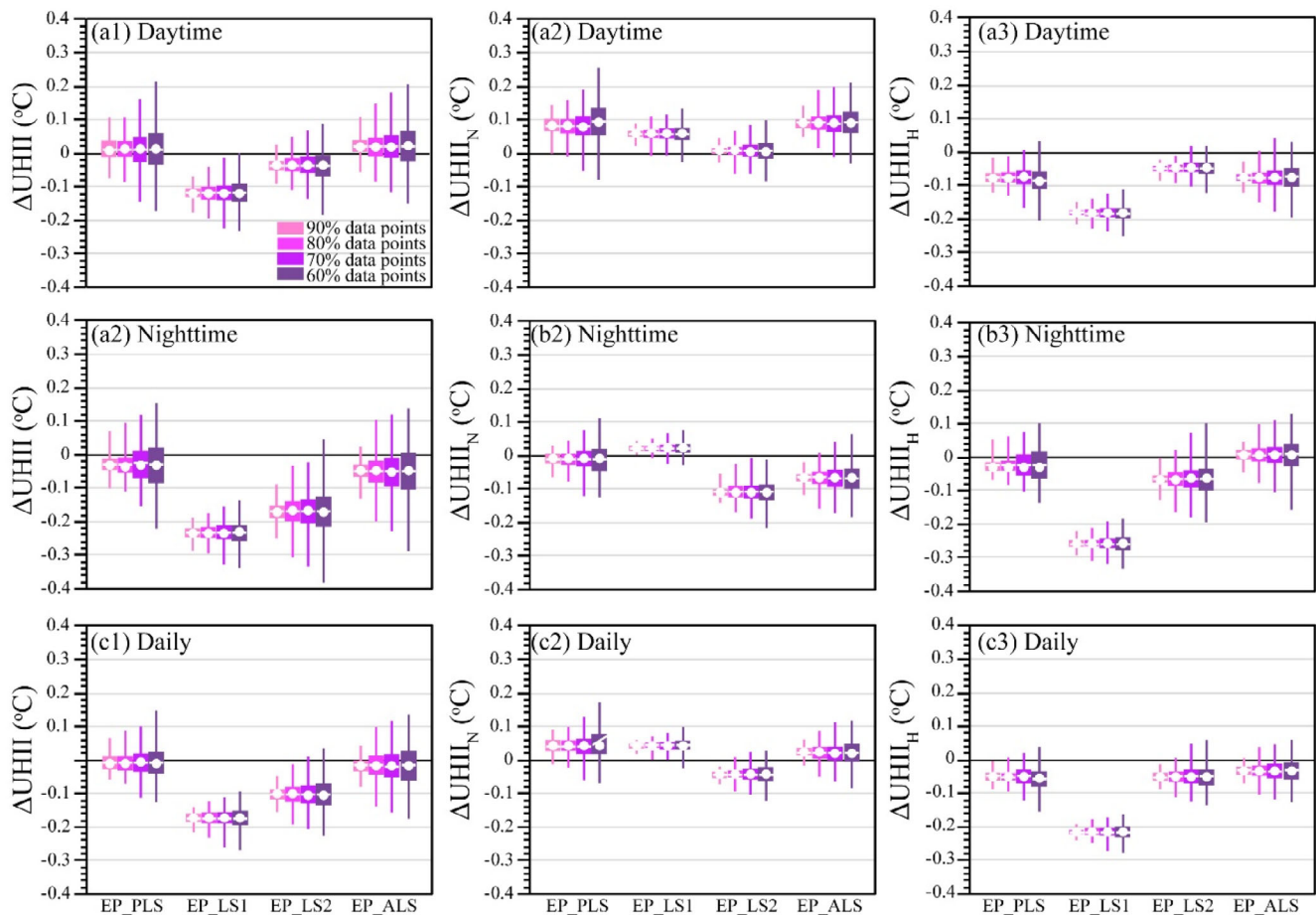
FIGURE 5 Box-plots of $\Delta UHII$ (a1–a3), $\Delta UHII_N$ (b1–b3), and $\Delta UHII_H$ (c1–c3) in each EP stage, which are recalculated with randomly sampled data points and 1,000 repetitions. The white dots and horizontal lines represent the median and mean values, respectively. The bottom of the vertical lines (the box) is the minimum (25 percentile), while the top is the maximum (75 percentile). For the case of "$x\%$ data points" ($x = 90, 80, 70,$ and 60), the samples for EP_PLS, EP_LS, EP_LS2, and EP_ALS are $22 \times x\%$, $56 \times x\%$, $40 \times x\%$, and $33 \times x\%$, respectively

randomly sampling the 90, 80, 70, and 60% data points from the $\Delta UHII$, $\Delta UHII_N$, and $\Delta UHII_H$ time series of each stage during EP with 1,000 repetitions. The results are shown in Figure 5, accompanied by occurrences among the 1,000 repetitions with significant ($p < .05$) values (Table S4). For the recalculated daytime, nighttime, and daily $\Delta UHII$ ($\Delta UHII_N$, and $\Delta UHII_H$) with different samples, it is evident that the values averaged over 1,000 repetitions are close (differences below 0.02°C) to each other in each EP stage, which implies that the local weather conditions have limited impact on the identified EP UHII changes. Based on occurrences with significant ($p < .05$) $\Delta UHII$ and $\Delta UHII_H$ among the 1,000 repetitions, we found that these occurrences are much less than 1,000 in EP_PLS, EP_LS2, and EP_ALS; however, they are almost equal to 1,000 in EP_LS1. Moreover, the occurrence with statistically significant ($p < .05$) $\Delta UHII_N$ during all EP stages is much less than 1,000. These findings indicate that local weather conditions have limited

influence on the statistical significance of the EP $\Delta UHII$. Hence, we confirm that the EP UHII changes are robust, particularly in EP_LS1 and EP_LS2, and thus could be attributed to the reduced human activities due to the COVID-19. Additionally, considering limited or no landcover changes around the utilized weather sites (Figures S1 and S2), the strict antivirus measures are responsible for the EP_LS1 and EP_LS2 UHII decreases.

4 | DISCUSSION

This study demonstrates an evident UHII decrease during the COVID-19 lockdown in Wuhan. The results are generally consistent with the findings of the COVID-19 lockdown impacts on UHII in other regions, which were examined using in situ observations, remote sensing datasets, and numerical simulations (Fujibe, 2020; Ali *et al.*, 2021; Alqasemi *et al.*, 2021; Kenawy *et al.*, 2021; Nakajima *et al.*, 2021;

8800 | International Journal of Climatology | RMetS
SHANLEI ET AL.

Shikwambana *et al.*, 2021; Jallu *et al.*, 2022; Liu *et al.*, 2022). For example, Fujibe (2020) compared the temperatures at the Tokyo station during the self-constrained period (i.e., the first half of 2020) with those of the unconstrained scenario. The latter was estimated based on a regression equation developed with data from 2015 to 2019 and temperatures at surrounding nonurban stations during the self-constrained period. He found that negative temperature anomalies were widely distributed in the Tokyo Metropolitan area during the self-constrained period, with a significant anomaly of $-0.49 \pm 0.19°C$ averaged during April–May in the central part of Tokyo. Using a regional climate model coupled with urban canopy and building energy models, Nakajima *et al.* (2021) found that the COVID-19 restrictions could reduce $0.13°C$ in the urban areas of Osaka, Japan. Additionally, our findings also concur with the response of UHII and urban temperatures on weekends and holidays (Forster and Solomon, 2003; Fujibe, 2010; Wu *et al.*, 2015; Zhang *et al.*, 2015a; 2015b; Ohashi *et al.*, 2016; Dou and Miao, 2017; Earl *et al.*, 2016; Bäumer and Voge, 2007). For instance, the reduction was between $0.20–0.25°C$ on weekends and holidays in Tokyo and between $0.10–0.20°C$ in Osaka (Fujibe, 2010). It ranged from 0.10 to $0.20°C$ in seven major cities of Australia (Earl *et al.*, 2016) and from 0.13 to $0.37°C$ in 12 cities in Germany (Bäumer and Voge, 2007). Therefore, the magnitude of UHII and urban temperature decreases varied across regions, which may be related to differences in methodology, anti-antivirus measures, and urban characteristics (e.g., dominant land cover types, urban form, population, economic development level, industrial activity, and climate background among regions; Ali *et al.*, 2021; Jia *et al.*, 2021; Kenawy *et al.*, 2021; Jallu *et al.*, 2022).

Some limitations in this study should also be noted. Wang and Zhang (2020) reported reductions of various aerosol emissions that did not exceed 50%, such as $PM_{2.5}$, PM_{10}, SO_2, and NO_2, over Wuhan during the COVID-19 lockdown, implying that more solar radiation would likely be absorbed by the land surface and then air temperature would likely increase over both urban and rural areas (e.g., Yang *et al.*, 2020a). However, due to differences in the thermal properties between the urban (mainly coved by various materials with increased heat storage capacity) and rural areas (mainly covered by natural land surfaces, for example, various vegetation), more heat would be stored by the urban areas and thus warming rates may be larger over urban areas, that is, increased UHII (Liu *et al.*, 2022). For example, Liu *et al.* (2022) pointed out that aerosol reductions caused by the suppressed residential activity only showed a 0.85% increase in UHII in six representative megacities in China during the lockdown period. Therefore, the identified UHII that decreases during the Wuhan lockdown are potentially underestimated due to the warming induced by the declined aerosols, and may be due to the reduced AH associated with human activities. Further investigations should quantify the contributions of the reduced AH and the effect of aerosol emissions on the UHII changes. We conducted visual comparisons of land cover between 2016 and 2020 at each weather site for reducing the impact of land cover changes; nevertheless, shifts in vegetation types, differences in soil moisture (especially in rural areas), and socio-economic development (e.g., lifestyle changes and adjustment of industry structure) were not considered in our study, and can potentially influence our findings (e.g., Husain *et al.*, 2014; Chapman *et al.*, 2018; Hoan *et al.*, 2018; Manoli *et al.*, 2020; Liu *et al.*, 2022).

Moreover, owing to the evident UHII differences among cites and diverse climate zones (Ren *et al.*, 2007; Yow, 2007; Zhou *et al.*, 2014; Li *et al.*, 2019; Jia *et al.*, 2021), how the UHII responds to the COVID-19 over the other cities and whether such responses differ among cities and/or among diverse climate zones needs to be studied further; however, we focused on only one city, deeming further investigations necessary.

5 | CONCLUSIONS

Based on observed air temperatures, we examined the impacts of the COVID-19 during January 1, 2020–May 31, 2020 on the Wuhan UHI effects relative to the baseline period of 2016–2019 and 2021. By dividing the selected period into four stages (i.e., EP_PLS, EP_LS1 with the strictest antivirus measures, EP_LS2 with the strict measures, and EP_ALS), we constructed four scenarios representing different intensities of human activities in Wuhan, and compared them to the corresponding stages of 2016–2019 and 2021, thereby estimating the UHII changes in each stage. Daytime, night-time, and daily UHII were consistently decreased in EP_LS1 and EP_LS2 stages, albeit with different rates; the largest ($<-0.12°C$ or $<-36\%$) and significant ($p < .05$) decreases appeared in EP_LS1. After removing the impact of the air temperature's natural variability, results showed that EP_LS1 and EP_LS2 still exhibited negative daytime, night-time, and daily UHII changes, with the largest ($<-0.18°C$ or $<-52\%$) and significant ($p < .05$) reductions in EP_LS1. Comparisons of $\Delta UHII_N$ and $\Delta UHII_H$ suggest that the reduced human activities should be responsible for the EP_LS1 and EP_LS2 UHII decreases. By randomly sampling data points, the impact of the weather conditions on the robustness of our findings were assessed in terms of magnitude and significance. We confirmed that weather conditions had limited impact and that the declined UHII values in EP_LS1 and EP_LS2

were mainly because of the strict antivirus measures, especially the significant reductions in EP_LS1. We showed that strict COVID-19 prevention and control measures not only had a positive effect on human health, but also evidently decreased the UHI effect.

This study elucidates the impact of the COVID-19 lockdown on the UHII, and constitutes an important reference for quantitatively understanding the role of human activities in the UHI effect and thus optimally managing and utilizing this effect. More importantly, the significant UHII reductions during the lockdown confirm that the human dynamics play a considerable role in urban climate, and more efforts should be devoted to explicitly including the human dynamics in climate/earth system models for better simulating and predicting urban and even local climate.

CONFLICT OF INTEREST

The authors declare no potential conflict of interest.

DATA AVAILABILITY STATEMENT

The authors have no authority to publish the used observational data (i.e., the observed hourly 2-m air temperature, and the data of daily electricity consumption over the Wuhan metropolitan area). However, if the readers are interesting in this study, please contact the corresponding author by email sun.s@nuist.edu.cn and the data can be supported by cooperation. The 30×30 m GlobeLand30 dataset of 2020 was from http://www. globallandcover.com. We thank all data developers, and their managers and funding agencies, whose work and support were invaluable. All the calculations and figure plots were using the software of Python, which has the functions that are free to obtain (https://python.org).

ORCID

Sun Shanlei https://orcid.org/0000-0002-7237-2722
Chen Haishan https://orcid.org/0000-0002-2403-3187

REFERENCES

Ali, G., Abbas, S., Oamer, F.M., Wong, M.S., Rasul, G., Irteza, S.M. and Shahzad, N. (2021) Environmental impacts of shifts in energy, emissions, and urban heat island during the COVID-19 lockdown across Pakistan. *Journal of Cleaner Production*, 291, 125806.

Alqasemi, A.S., Hereher, M.E., Kaplan, G., al-Quraishi, A.M.F. and Saibi, H. (2021) Impact of COVID-19 lockdown upon the air quality and surface urban heat island intensity over The United Arab Emirates. *Science of the Total Environment*, 767, 144330.

Arnfield, A.J. (2003) Two decades of urban climate research: a review of turbulence, exchanges of energy and water, and the urban heat island. *International Journal of Climatology*, 23, 1–26.

Bäumer, D. and Voge, B. (2007) An unexpected pattern of distinct weekly periodicities in climatological variables in Germany. *Geophysical Research Letters*, 34(3), 10–13.

Beckage, B., Gross, L.J., Lacasse, K., Carr, E., Metcalf, S.S., Winter, J.M., Howe, P.D., Fefferman, N., Franck, T., Zia, A., Kinzig, A. and Hoffman, F.M. (2018) Linking models of human behavior and climate alters projected climate change. *Nature Climate Chenge*, 8(1), 79–84.

Chapman, S., Thatcher, M., Salazar, A., Watson, J.E.M. and McAlpine, C.A. (2018) The effect of urban density and vegetation cover on the heat island of a subtropical city. *Journal of Applied Meteorology and Climatology*, 57(11), 2531–2550.

Chen, J., Ban, Y. and Li, S. (2014) China: open access to earth land-cover map. *Nature*, 514(7523), 434.

Chen, S., Yang, J., Yang, W., Wang, C. and Bärnighausen, T. (2020) COVID-19 control in China during mass population movements at new year. *Lancet*, 395, 764–766.

China Internet Information Center. (2020) *China's Wuhan takes unprecedented measures to curb novel coronavirus*. Available at: www.china.org.cn/china/Off_the_Wire/2020-01-23/content_75643971.htm.

Chistoforou, C.S., Salmon, L.G., Hannigan, M.P., Solomon, P.A. and Cass, G.R. (2000) Trends in fine particle concentration and chemical composition in southern California. *Journal of the Air & Waste Management Association*, 50(1), 43–53.

Donges, J.F., Heitzig, J., Barfuss, W., Wiedermann, M., Kassel, J.A., Kittel, T., Kolb, J.J., Kolster, T., Müller-Hansen, F., Otto, I.M., Zimmerer, K.B. and Lucht, W. (2020) Earth system modeling with endogenous and dynamic human societies: the Copan: core open world-earth modeling framework. *Earth System Dynamics*, 11(2), 395–413.

Dou, J. and Miao, S. (2017) Impact of mass human migration during Chinese New Year on Beijing urban heat island. *International Journal of Climatology*, 37(11), 4199–4210.

Earl, N., Simmonds, I. and Tapper, N. (2016) Weekly cycles in peak time temperatures and urban heat island intensity. *Environmental Research Letters*, 11, 074003.

Fan, H. and Sailor, D.J. (2005) Modeling the impacts of anthropogenic heating on the urban climate of Philadelphia: a comparison of implementations in two PBL schemes. *Atmospheric Environment*, 39, 73–84.

Feng, J.M., Wang, Y. and Ma, Z. (2012) Simulating the regional impacts of urbanization and anthropogenic heat release on climate across China. *Journal of Climate*, 25, 7187–7203.

Forster, P.M.F. and Solomon, S. (2003) Observations of a "weekend effect" in diurnal temperature range. *Proceedings of the National Academy of Sciences of the United States of America*, 100(20), 11225–11230.

Fujibe, F. (2010) Day-of-the-week variations of urban temperature and their long-term trends in Japan. *Theoretical and Applied Climatology*, 102(3), 393–401.

Fujibe, F. (2020) Temperature anomaly in the Tokyo metropolitan area during the COVID-19 (coronavirus) self-restraint period. *Scientific Online Letters on the Atmosphere*, 16, 175–179.

Gedzelman, S.D., Austin, S., Cermak, R., Stefano, N., Partridge, S., Quesenberry, S. and Robinson, D.A. (2013) Mesoscale aspects of the urban heat island around New York City. *Theoretical & Applied Climatology*, 75, 29–42.

Goldberg, D.L., Anenberg, S.C., Griffin, D., McLinden, C.A., Lu, Z. and Streets, D.G. (2020) Disentangling the impact of the COVID-19 lockdowns on urban NO_2 from natural variability. *Geophysical Research Letters*, 47, e2020GL089269.

Hoan, N.T., Liou, Y.-A., Nguyen, K.-A., et al. (1965) Assessing the effects of land-use types in surface urban Heat Islands for developing comfortable living in Hanoi City. *Remote Sensing*, 2018, 10.

Hoan, N.T., Liou, Y.-A., Nguyen, K.-A., Sharma, R.C., Tran, D.-P., Liou, C.-L. and Cham, D.D. (2018) *Assessing the effects of land-use types in surface urban Heat Islands for developing comfortable living in Hanoi City*. Remote Sensing.

Hubei Government. (2020). *No 9 notification from prevention and control headquarters for epidemic in Wuhan* (in Chinese). Available at: https://www.hubei.gov.cn/zhuanti/2020/gzxxgzbd/zxtb/202001/t20200125_2014946.shtml.

Husain, S.Z., Bélair, S. and Leroyer, S. (2014) Influence of soil moisture on urban microclimate and surface-layer meteorology in Oklahoma City. *Journal of Applied Meteorology and Climatology*, 53(1), 83–98.

Jallu, S.B., Shaik, R.U., Srivastav, R. and Pignatta, G. (2022) Assessing the effect of COVID-19 lockdown on surface urban heat island for different land use/cover types using remote sensing. *Energy Nexus*, 5, 100056.

Jia, W., Ren, G., Yu, X., Zhang, Y. and Zhang, P. (2021) Difference of urban heat island effect among representative cities of different climatic zones over eastern China monsoon region. *Climatic and Environmental Research*, 26(5), 569–582 (in Chinese).

Kenawy, A.M.E., Lopez-Moreno, J.I., McCabe, M., Domínguez-Castro, F., Peña-Angulo, D., Gaber, M.I., Alqasemi, A.S., Kindi, K.M.A., Al-Awadhi, T., Hereher, M.E., Robaa, S.M., Nasiri, N.A. and Vicente-Serrano, S.M. (2021) The impact of COVID-19 lockdowns on surface urban heat Island changes and air-quality improvements across 21 major cities in the Middle East. *Environmental Pollution*, 288, 17802.

Kistler, R., Kalnay, E., Collins, W., Saha, S., White, G., Woollen, J., Chelliah, M., Ebisuzaki, W., Kanamitsu, M., Kousky, V., van den Dool, H., Jenne, R. and Fiorino, M. (2001) The NCEP-NCAR 50-year reanalysis: monthly means CD-ROM and documentation. *Bulletin of the American Meteorological Society*, 82, 247–268.

Li, D., Liao, W., Rigden, A., Liu, X., Wang, D., Malyshew, S. and Shevliakova, E. (2019) Urban heat island: aerodynamics or imperviousness? *Science Advances*, 5(4), eaau4299.

Liu, Z., Lai, J., Zhan, W., Bechtel, B., Voogt, J., Quan, J., Hu, L., Fu, P., Huang, F., Li, L., Guo, Z. and Li, J. (2022) Urban heat islands significantly reduced by COVID-19 lockdown. *Geophysical Research Letters*, 49, e2021.

Magee, N., Curtis, J. and Wendler, G. (1999) The urban heat island effect at Fairbanks, Alaska. *Theoretical & Applied Climatology*, 64, 39–47.

Manoli, G., Fatichi, S., Bou-Zeid, E. and Katul, G.G. (2020) Seasonal hysteresis of surface urban heat islands. *Proceedings of the Natural Academy of Sciences of the United States of America*, 117(13), 7082–7089.

Miyazaki, K., Bowman, K., Sekiya, T., Jiang, Z., Chen, X., Eskes, H., Ru, M., Zhang, Y. and Shindell, D. (2020) Air quality response in China linked to the 2019 novel coronavirus (COVID-19) lockdown. *Geophysical Research Letters*, 47, e2020GL089252.

Nakajima, K., Takane, Y., Kikegawa, Y., Furuta, Y. and Takamatsu, H. (2021) Human behaviour change and its impact on urban climate: restrictions with the G20 Osaka Summit and COVID-19 outbreak. *Urban Climate*, 35, 100728.

Narumi, D., Kondo, A. and Shimoda, Y. (2009) Effects of anthropogenic heat release upon the urban climate in a Japanese megacity. *Environmental Research*, 109, 421–431.

Ohashi, Y., Ihara, T., Kikegawa, Y. and Sugiyama, N. (2016) Numerical simulations of influence of heat island countermeasures on outdoor human heat stress in the 23 wards of Tokyo, Japan. *Energy and Buildings*, 114, 104–111.

Oke, T.R. (1982) The energetic basis of the urban heat island. *Quarterly Journal of the Royal Meteorological Society*, 108, 1–24.

Oleson, K. (2012) Contrast between urban and rural climate in CCSM1 CMIP5 climate change scenarios. *Journal of Climate*, 25(5), 1390–1412.

Oleson, K.W., Bonan, G.B., Feddema, J. and Jackson, T. (2011) An examination of urban heat island characteristics in a global climate model. *International Journal of Climatology*, 31(12), 1848–1865.

Raj, S., Pau, S.K., Chakraborty, A. and Kuttippurath, J. (2020) Anthropogenic forcing exacerbating the urban heat islands in India. *Journal of Environmental Management*, 257, 110006.

Ren, G.Y., Chu, Z.Y., Chen, Z.H. and Ren, Y.Y. (2007) Implications of temporal change in urban heat island intensity observed at Beijing and Wuhan stations. *Geophysical Research Letters*, 34, L057711.

Shi, X. and Brasseur, G.P. (2020) The response in air quality to the reduction of Chinese economic activities during the COVID-19 outbreak. *Geophysical Research Letters*, 47, e2020GL088070.

Shikwambana, L., Kganyago, M. and Mhangara, P. (2021) Temporal analysis of changes in anthropogenic emissions and urban heat islands during COVID-19 restrictions in Gauteng Province, South Africa. *Aerosol and Air Quality Research*, 21(9), 200437.

Tian, H., Liu, Y., Li, Y., Wu, C.H., Chen, B., Kraemer, M.U.G., Li, B., Cai, J., Xu, B., Yang, Q., Wang, B., Yang, P., Cui, Y., Song, Y., Zheng, P., Wang, Q., Bjornstad, O.N., Yang, R., Grenfell, B.T., Pybus, O.G. and Dye, C. (2020) An investigation of transmission control measures during the first 50 days of the COVID-19 epidemic in China. *Science*, 368, 638–642.

Tong, H., Liu, H.Z., Sang, J.G. and Hu, F. (2004) The impact of urban anthropogenic heat on Beijing heat environment. *Climatic and Environmental Research*, 9(3), 409–421 (in Chinese).

Turner, A.J., Kim, J., Fitzmaurice, H., Newman, C., Worthington, K., Chan, K., Wooldridge, P., Köehler, P., Frankenberg, C. and Cohen, R. (2020) Observed impacts of COVID-19 on urban CO_2 emissions. *Geophysical Research Letters*, 47, e2020GL090037.

Varentsov, M., Konstantinov, P., Baklanov, A., Esau, I., Miles, V. and Davy, R. (2018) Anthropogenic and natural drivers of a strong winter urban heat island in a typical Arctic city. *Atmospheric Chemistry & Physics*, 18, 17573–17587.

Wang, X. and Zhang, R. (2020) How did air pollution change during the COVID-19 outbreak in China? *Bulletin of the American Meteorological Society*, 101(10), E1645–E1652.

Word Health Organization (WHO). (2021) *WHO Coronavirus Disease (COVID-19) dashboard*. Available at: https://covid19.who.int/.

Wu, H., Wang, T., Riemer, N., Chen, P., Li, M. and Li, S. (2017) Urban heat island impacted by fine particles in Nanjing, China. *Scientific Reports*, 7, 11422.

Wu, L., Zhang, J. and Shi, C. (2015) Mass human migration and the urban heat island during the Chinese new year holiday: a case study in Harbin City, northeast China. *Atmospheric and Oceanic Science Letters*, 8(2), 63–66.

Yang, P. and Liu, W.D. (2013) Evaluating the quality of meteorological data measured at automatic weather stations in Beijing during 1998–2010. *Advances in Meteorological Science and Technology*, 3(6), 27–34 (in Chinese).

Yang, P., Liu, W.D., Zhong, J.Q. and Yang, J. (2011) Evaluating the quality of temperature measured at automatic weather stations in Beijing. *Journal of Applied Meteorological Science*, 22, 706–715 (in Chinese).

Yang, P., Ren, G. and Hou, W. (2019) Impact of daytime precipitation duration on urban heat island intensity over Beijing City. *Urban Climate*, 28, 100463.

Yang, Y., Ren, L., Li, H., Wang, H., Wang, P., Chen, L., Yue, X. and Liao, H. (2020a) Fast climate response to aerosol emission reductions during the COVID-19 pandemic. *Geophysical Research Letters*, 47, e2020GL089788.

Yang, Y., Zheng, Z., Yim, S.Y.L., Roth, M., Ren, G., Gao, Z., Wang, T., Li, Q., Shi, C., Ning, G. and Li, Y. (2020b) PM2.5 pollution modulates wintertime urban heat island intensity in the Beijing-Tianjin-Hebei megalopolis, China. *Geophysical Research Letters*, 47, e2019GL084288.

Yow, D.M. (2007) Urban heat island: observations, impacts, and adaptation. *Geography Compass*, 1(6), 1227–1251.

Zhang, J., Wu, L., Yuan, F., Dou, J. and Miao, S. (2015a) Mass human migration and Beijing's urban heat island during the Chinese new year holiday. *Science Bulletin*, 60(11), 1038–1041.

Zhang, L., Ren, G. and Ren, Y. (2015b) Identification of urban effect on a single extreme high temperature event. *Climatic and Environmental Research*, 20(2), 167–176 (in Chinese).

Zhou, D., Zhao, S., Liu, S., Zhang, L. and Zhu, C. (2014) Surface urban heat island in China's 32 major cities: spatial patterns and drivers. *Remote Sensing of Environment*, 152, 51–61.

SUPPORTING INFORMATION

Additional supporting information can be found online in the Supporting Information section at the end of this article.